Magnetocaloric Effects and the Angular Variation of the Magnetic Phase Diagram of Antiferromagnetic GdAlO$_3$

Keith W. Blazey, Heinrich Rohrer, and Ronald Webster[*]

IBM Zurich Research Laboratory, 8803 Rüschlikon, Zurich, Switzerland

(Received 1 April 1971)

The isothermal magnetic phase diagram of GdAlO$_3$ has been measured, and a molecular field analysis yielded the following values of the coupling constants: isotropic intersublattice coupling $J_1 = 0.722$ K, isotropic intrasublattice coupling $J_2 = 0.051$ K, anisotropic intersublattice coupling $K_1 = 0.0438$ K, anisotropic intrasublattice coupling $K_2 = 0.036$ K, and crystal field anisotropy constant $L_0 = -0.132$ K. The magnetic phase boundaries calculated with these molecular field constants agreed with experiment except for the spin-flop transition near the triple point. This transition has been studied in detail as a function of the angle between the easy axis and the applied field. A first-order phase transition is found only within a critical angle as predicted theoretically. This critical angle also varies with sample shape owing to its dramatic dependence on demagnetization. The striking differences between the isothermal and the previously reported adiabatic phase diagrams are attributed to magnetocaloric cooling. The cooling on adiabatic magnetization of an antiferromagnet in its antiferromagnetic phase is calculated within the molecular field approximation (MFA) and is found to agree with this experiment and others. A comparable cooling, not predicted by the MFA, is observed for fields applied perpendicular to the easy axis.

I. INTRODUCTION

Magnetic phase diagrams of antiferromagnets have recently been studied both theoretically[1-5] and experimentally.[6-15] The phase diagram of a uniaxial antiferromagnet with the magnetic field applied along the easy axis of magnetization is drawn schematically in Fig. 1. The paramagnetic (PM) state is separated from the spin-flop (FL) state and the antiferromagnetic (AF) state by the two second-order phase boundaries, FL-PM and AF-PM, respectively. The AF phase is separated from the FL phase by a first-order phase transition which meets the PM phase boundary in the triple point T_t. Associated with this first-order phase transition are the stability limits of the FL phase (FL-AF) and the AF phase (AF-FL) with the thermodynamic phase boundary lying between them. The field at which the system undergoes the first-order phase transition is usually referred to as the spin-flop field.

The magnetic phase diagram and its dependence on the direction of the magnetic field can be used to determine the magnetic coupling constants.[8,9] In this paper we concentrate in more detail on three aspects of the phase diagram, namely, the temperature dependence of the critical fields, the dependence of the spin-flop transition on the direction of the applied field, and the apparent phase-boundary shifts caused by the magnetocaloric effect. Experimentally, the magnetic phase boundaries are traced out by peaks or discontinuities in the ultrasonic attenuation,[13] specific heat,[11,12] and magnetization or differential magnetization.[8,9]

In the present investigations the transition fields were located by peaks of the differential magnetization. The experimental results are interpreted in terms of a molecular field approximation (MFA), which not only gives a satisfactory qualitative description of the experiment, but also a surprisingly good quantitative description of many of the results. However, the isotropic field dependence of the sublattice magnetizations observed in the FL state at high temperatures and the critical behavior of the differential magnetization close to the phase boundaries are beyond MFA.

The angular dependence of the phase diagram has been investigated previously,[8] but quantitative results were reported only for the PM phase boundary. These experiments also showed a rapid decrease of the maximum of the differential magnetization at the spin-flop transition if the applied field was tilted away from the easy axis of magnetization. Chepurnykh[3] and Rohrer and Thomas[4] have shown that at $T = 0$ K a first-order spin-flop transition exists only for angles between the easy axis and the applied field less than a critical angle which is of the order anisotropy/exchange. For angles larger than this critical angle the sublattice magnetizations turn continuously from an antiferromagneticlike configuration into a spin-flop-like configuration. It was later shown[5] that this critical angle decreases with increasing temperature and vanishes at the triple point. For finite angles less than the critical angle, the first-order phase transition between the AF state and the FL state is no longer connected to the PM phase boundary but ends in a critical point. Between this critical point and the kink in the PM
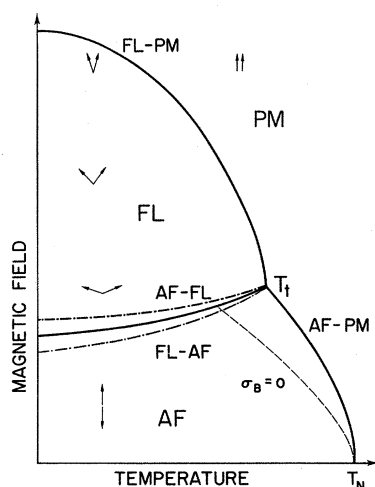
FIG. 1. Schematic phase diagram of a uniaxial antiferromagnet for the field applied along the easy axis. At the triple point T_t all three phases coexist. Broken line $\sigma_B = 0$ is not a phase boundary; its significance is explained in conjunction with Eq. (3a).

phase boundary, the sublattice magnetizations turn continuously but also sufficiently fast to induce a substantial change of magnetization in a small field interval. Such a pseudotransition is not easy to distinguish from a real transition. Since the question of the existence or nonexistence of a phase transition is an important one in the experiments related to soft modes, domain effects, etc., we have studied this problem and determined the critical angle as a function of temperature. Preliminary results of this investigation have been reported elsewhere.[14]

The magnetic phase diagram for static fields along the easy axis of magnetization is different from the one measured previously[8] with pulsed fields. The difference of these phase diagrams is attributed to adiabatic cooling in the AF state on magnetization by fast field pulses.[15] The possibility of adiabatic cooling has already been discussed by Kurti[16] for the case of antiferromagnetic ordering at very low temperatures in the classical salts used for adiabatic demagnetization, and by Wolf[17] for paramagnetic ions with a crystal-field-induced nonmagnetic ground state. More recently, the cooling on magnetization of antiferromagnets[10,12] and ferrimagnets[18] has been observed by measuring the temperature of the sample on magnetizing or the field dependence of the specific heat. Here we give a more detailed and quantitative analysis of the magnetocaloric effect based on a molecular field calculation and compare the results with our phase-diagram measurements on GdAlO$_3$ and other experiments.

Finally, we discuss briefly the temperature

dependence of the PM boundary near the Néel temperature. In the isothermal case, molecular field behavior is observed. In the adiabatic case, the phase boundary represents the temperature dependence of the order parameter and shows critical behavior similar to that found in other antiferromagnets.

Before reverting to the problems just outlined, it is useful to write down a few molecular field expressions which will be used throughout the paper and which are derived in more detail in Ref. 5. The free energy of an antiferromagnet with N spins S per sublattice is given by

$$F = N\{S^2[J_1\sigma_A\sigma_B\cos(\alpha - \beta) + \tfrac{1}{2}J_2(\sigma_A^2 + \sigma_B^2)$$
$$+ K_1\sigma_A\sigma_B\cos\alpha\cos\beta + \tfrac{1}{2}K_2(\sigma_A^2\cos^2\alpha + \sigma_B^2\cos^2\beta)]$$
$$- g\mu_B\, SH[\sigma_A\cos(\alpha - \psi) + \sigma_B\cos(\beta - \psi)]$$
$$- T[s(\sigma_A) + s(\sigma_B)]\}, \qquad (1)$$

where α, β, and ψ are the angles of sublattice A, sublattice B, and the magnetic field H with the easy axis of magnetization as explained in Fig. 2; σ_A and σ_B, the average values of the spins of sublattice A and sublattice B normalized to 1 (i.e., $\sigma_A = \langle S_A \rangle / S$, where S_A is a spin on sublattice A); J_1 and K_1, the intersublattice; J_2 and K_2, the intrasublattice isotropic and anisotropic coupling constants; T, the temperature; and $s(\sigma_A)$ and $s(\sigma_B)$, the entropies per spin of sublattices A and B, respectively. The crystal field effects in their simplest form further contribute to the K_2-type anisotropy. In second order, the crystal field anisotropy takes the more complicated form[5]

$$\tfrac{1}{2} L_0\left[l(\sigma_A)\sigma_A^2(\cos^2\alpha - \tfrac{1}{3}) + l(\sigma_B)\sigma_B^2(\cos^2\beta - \tfrac{1}{3})\right], \qquad (1')$$

where $l(\sigma)$ varies as σ for $\sigma \to 1$ and is constant for $\sigma \to 0$ with $l(0) = \tfrac{3}{5} l(1)(2S + 3)/(2S + 2)$. For $\sigma \approx 1$ or $\sigma \approx 0$ this L-type anisotropy can be treated similar to the K_2-type anisotropy except that the anisotropy constant is different in the limits $\sigma = 1$ and 0. At intermediate values of σ, the numerical calculations are unduly complicated by the σ de-
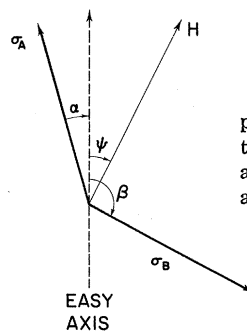

FIG. 2. Angles defining the position of the sublattice magnetizations in a field applied at an angle to the easy axis. Here β and ψ are positive and α negative.

pendence of l without changing the results appreciably. Therefore, if not stated otherwise, we include L-type anisotropy only in calculations related to properties at $T = 0$ K ($\sigma \approx 1$) or for T not much below T_N and small fields (σ small). Further contained in the K_1- and K_2-type anisotropies is the shape anisotropy caused by the demagnetizing fields. For effects such as superheating and supercooling and angular dependence of the spin-flop transition, this type of anisotropy can be the dominant part. For the different anisotropies, with the signs given in Eq. (1), to favor the easy direction, K_1 has to be positive and K_2 and L_0 negative. The sublattice entropies are of the form

$$ds(\sigma)/d\sigma = -B^{-1}(\sigma) \ , \tag{2}$$

where $B^{-1}(\sigma)$ is the inverse Brillouin function for spin S.

The equilibrium positions of the sublattice magnetizations are found by putting the derivatives of F with respect to α, β, σ_A, and σ_B equal to zero. One obtains for the field applied along the easy axis the following results:

Antiferromagnetic state ($\alpha = 0$, $\beta = \pi$):

$$\sigma_A = B\{(S^2/T)[-(J_2+K_2)\sigma_A + (J_1+K_1)\sigma_B$$
$$+(g\mu_B/S)H]\} = B(X_A),$$
$$\sigma_B = B\{(S^2/T)[-(J_2+K_2)\sigma_B + (J_1+K_1)\sigma_A$$
$$-(g\mu_B/S)H]\} = B(X_B). \tag{3a}$$

Flop state ($\sigma_A = \sigma_B = \sigma$, $\alpha = -\beta = \varphi$):

$$\sigma = B[(S^2/T)(J_1-J_2)\sigma] = B(X_F),$$
$$\cos\varphi = (g\mu_B/S)H/[(2J_1+K_1+K_2)\sigma]. \tag{3b}$$

Paramagnetic state ($\sigma_A = \sigma_B = \sigma$, $\alpha = \beta = 0$):

$$\sigma = B\{(S^2/T)[-(J_1+J_2+K_1+K_2)\sigma + (g\mu_B/S)H]\}$$
$$= B(X_P). \tag{3c}$$

And for fields perpendicular to the easy direction:

Flop state:

$$\sigma = B[(S^2/T)(J_1+K_1-J_2-K_2)\sigma] \ ,$$
$$\sin\varphi = (g\mu_B/S)H/[(2J_1+K_1-K_2)\sigma] \ . \tag{3d}$$

Paramagnetic state:

$$\sigma = B\{(S^2/T)[(g\mu_B/S)H - \sigma(J_1+J_2)]\} \ . \tag{3e}$$

For the antiferromagnetic state there also exist solutions with $\alpha = \beta = 0$ in the region to the right of the line $\sigma_B = 0$ in Fig. 1. Equations (3a) also account for these states if we let σ_B assume negative values.

An equilibrium state is stable as long as all the eigenvalues of the symmetric matrix formed by the second derivatives of F with respect to σ_A, σ_B, α, and β are positive. The eigenvector belonging to the first eigenvalue to become zero characterizes the type of instability of that state. It is found for fields along the easy axis that the system becomes unstable with respect to the following deviations and restrictions:

Along AF-PM,

$$\delta\sigma_A = -\delta\sigma_B \ , \qquad \delta\alpha = \delta\beta = 0 \ . \tag{4a}$$

Along FL-PM,

$$\delta\sigma_A = \delta\sigma_B = 0 \ , \qquad \delta\alpha = -\delta\beta \ . \tag{4b}$$

Along AF-FL,

$$\delta\sigma_A = \delta\sigma_B = 0, \quad |\delta\alpha\sigma_A| < |\delta\beta\sigma_B| \ . \tag{4c}$$

Along FL-AF,

$$\delta\sigma_A = -\delta\sigma_B, \qquad \delta\alpha = \delta\beta. \tag{4d}$$

For fields applied perpendicular to the easy axis the instability along the whole PM boundary is the same as (4b). Finally, we write down a few useful expressions for selected points in the H-T plane in terms of the molecular field constants J, K, and L:

Néel temperature:

$$T_N = \tfrac{1}{3}S(S+1)(J_1+K_1-J_2-K_2-\tfrac{4}{9}L_0). \tag{5a}$$

Paramagnetic Curie-Weiss temperature defined by $\chi_{||} = C/(T-\theta_{||})$:

$$\theta_{||} = -\tfrac{1}{3}S(S+1)(J_1+K_1+J_2+K_2+\tfrac{4}{9}L_0) \ . \tag{5b}$$

Triple point [to first order in $(T_N - T_t)/T_N$]:

$$T_t = T_N - \tfrac{3}{2}(T_N-T_3) \ , \tag{5c}$$

where

$$T_3 = \tfrac{1}{3}S(S+1)(J_1-J_2+\tfrac{2}{9}L_0) \tag{5d}$$

is the temperature obtained by extrapolating the FL-PM instability curve to $H = 0$.

Instability fields[4] at $T = 0$ K: (a) H parallel to easy axis:

$$H(\text{FL-PM}) = H_{c2}^{||} = A(2J_1+K_1+K_2+L_0) \ , \tag{6a}$$
$$H(\text{AF-FL}) = H_{sh} = A[(K_1-K_2-L_0)$$
$$\times(2J_1+K_1-K_2-L_0)]^{1/2}, \tag{6b}$$
$$H(\text{FL-AF}) = H_{sc} = A(2J_1+K_1+K_2+L_0)$$
$$\times[(K_1-K_2-L_0)/(2J_1+K_1-K_2-L_0)]^{1/2}, \tag{6c}$$

and the thermodynamical spin-flop field

$$H_{th} = A[(K_1-K_2-L_0)(2J_1+K_1+K_2+L_0)]^{1/2}$$

$$= (H_{sh} H_{sc})^{1/2} \ . \tag{6d}$$

(b) H perpendicular to easy axis:

$$H(\text{FL-PM}) = H_{c2}^{\perp} = A(2J_1 + K_1 - K_2 - L_0) \ , \tag{6e}$$

where the J's, K's, and L_0 are measured in units of K, H in kOe, and $A = S/g\mu_B = 14.888 S/g$.

These equations have been derived for uniaxial anisotropy. They are, however, also valid for orthorhombic anisotropy, as long as the applied field is kept in a plane perpendicular to the hard direction. Then the equilibrium positions of the sublattices remain in the plane of the easy axis and applied field, and the anisotropy in the hard direction does not appear in the above equations. The anisotropy in the hard direction plays a vital role, however, in the dynamic properties.

II. EXPERIMENT

The differential magnetization measurements were carried out on flux-grown single crystals[19] of GdAlO$_3$ cut into cylinders and a disk. The cylinders were up to 14 mm long with diameters of about 0.6 mm, and the disk was 0.05 mm thick and 3 mm in diameter. The demagnetizing field in the direction of the external field at saturation magnetization varied between 20 and 60 Oe for the cylinders and was 250 Oe in the case of the disk. In the following, the corrected fields are quoted. The Néel temperatures of the different samples agreed within the experimental accuracy and was $T_N = 3.875 \pm 0.005$ K. Geller and Bala[20] reported that GdAlO$_3$ has an orthorhombic structure. Consequently GdAlO$_3$ is not perfectly uniaxial in its magnetic properties.[21] The easy axis is the orthorhombic b axis and the hardest direction is the a axis, with the c axis intermediate. Only for fields applied in the bc plane do the spins flop in the plane of the easy axis and applied field. In this case the results may be compared with the molecular field theory of a uniaxial antiferromagnet and the orthorhombicity of the anisotropy neglected. Therefore, the cylinders used to determine the angular variation of the phase diagram were cut for each angle between the easy axis and applied field in the bc plane, with the cylinder axis in the direction of the applied field. The cylinders and the disk were oriented with x rays, so that the angle between the easy axis and applied field was known to $\pm 0.3°$. For a cylinder aligned along the easy axis with this accuracy of orientation, the narrowest spin-flop transition observed was less than 10 Oe at 10 kOe.

The susceptibility was measured by the mutual-inductance method[22] in the static field of a superconducting solenoid, the variable frequency field being supplied by a separate tickling-field coil.

Inside the tickling-field coil the pick-up coil with the sample and the compensation coil were mounted side by side. This arrangement allowed better compensation than the usual method with the two coils on top of each other. Also, for accurate compensation, the sample could be moved in and out of the pick-up coil at any temperature. The tickling field was about 1 Oe and its useful frequency range between 15 cps and 30 kcps.

III. RESULTS

A. Susceptibility and Phase Diagram

The susceptibility measured by the mutual-inductance method is not necessarily the isothermal susceptibility. Only if the spin system is coupled strongly enough to a large heat reservoir, such that entropy can be completely exchanged between the two within a cycle of the tickling field, is the isothermal susceptibility measured. The spin-lattice relaxation is usually fast enough ($\sim 10^{-6}$ sec) to keep the spin system and the lattice in thermal equilibrium up to tickling frequencies of many kcps even at low temperatures. But as the temperature is decreased the thermal capacity of the lattice becomes negligible and the surroundings have to act as the heat reservoir for the spin system. The thermal relaxation of our cylindrical samples was such that only measurements carried out at frequencies below 50 cps could be considered isothermal.

The measured susceptibility as a function of applied field for two cases is shown in Fig. 3. Two second-order phase transitions into the PM phase are clearly seen by their characteristic discontinuities in the susceptibility at X and Z. For temperatures above the triple point this transition is from the AF into the PM phase, whereas below T_t it is from the FL into the PM phase. Also, below T_t a peak is observed in the susceptibility showing a first-order phase transition due to the AF-FL transition, where the magnetization increases discontinuously. The different forms of the curves at X and Y clearly show this difference in the order of the AF-PM and AF-FL phase transitions.

The peak at the AF-FL transition has a finite width due to inhomogeneities of the bulk magnetic properties and demagnetizing fields, and consequently a finite height. In the case of isothermal susceptibility measurements (low-frequency tickling fields) the area under the susceptibility peak is equal to the jump in magnetization; in the adiabatic case (high-frequency tickling fields), however, the area under the peak is substantially reduced owing to the different magnetic field dependence of the isentropes and isotherms discussed in more detail later.
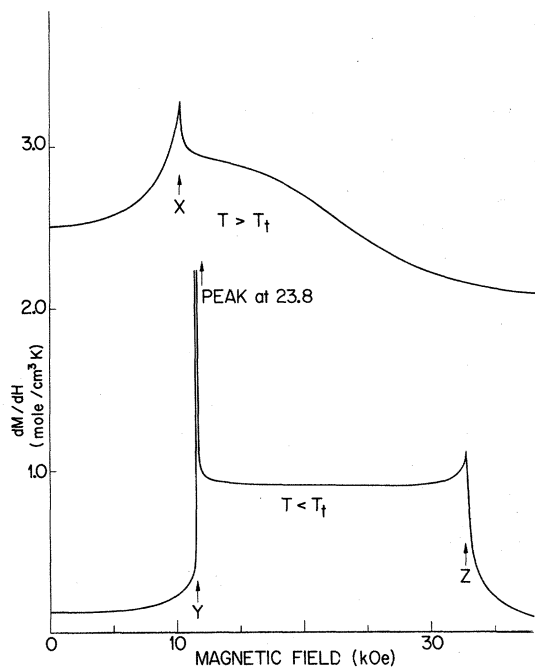
FIG. 3. Molar susceptibility of $GdAlO_3$ as a function of applied field measured with a tickling field of 2 Oe at 15 cps. Zero of the upper curve is displaced 2.0 vertically for clarity. (a) $T_t < T = 3.2$ K. Discontinuity at 10.2 kOe is due to the AF-PM phase transition. (b) $T_t > T = 1.48$ K. Peak at 11.3 kOe indicates the first-order spin-flop transition, and the abrupt drop at 32.4 kOe locates the FL-PM phase transition.

An easily measurable hysteresis is expected according to the antiferromagnetic resonance data,[23] for example, at $T = 2.3$ K, $\Delta H \approx 1240$ Oe for a cylinder with easy axis along the cylinder axis, but none was observed. That hysteresis is not observed seems to be quite general for the spin-flop transition, and to our knowledge neither has it been found in other antiferromagnets.[24] Thus the observed peak in the susceptibility is taken to locate the thermodynamical phase boundary between the AF and FL states.

Besides these abrupt changes in the susceptibility at the phase transitions, the more gentle field dependence between the phase transitions is also of interest. In the AF phase the susceptibility is far from being field independent. The gain of Zeeman energy at the spin-flop field H_{c1} is considerably more than the usually stated $\frac{1}{2}\chi_{||} H_{c1}^2$, where $\chi_{||}$ is the zero-field parallel susceptibility, thus rendering expressions for H_{c1} containing the zero-field susceptibility rather questionable.

In the FL state the susceptibility is nearly field and temperature independent both isothermally and adiabatically. This is in agreement with the molecular field approximation where the susceptibility

is due to the decreasing angle between the sub-lattice magnetizations. Within the MFA this susceptibility remains almost constant even if the sublattice magnetization does change, because the angle between the sublattices will change according to the changed molecular field.

Just below the FL-PM phase boundary the susceptibility increases logarithmically with H: $dM/dH = A + B \ln(H_{c2} - H)$. Jacobs and Silverstein[25] also found an increase in the transverse susceptibility prior to the FL-PM phase transition in EuTe and $CoCl_2$. This increase was attributed to zero-point reductions but the agreement with the theory of Kanamori and Yosida[26] was not good.

A plot of the critical fields shown in Fig. 3 against temperature yields the isothermal phase diagram. This is done in Fig. 4 for the fields applied parallel and perpendicular to the easy axis. This phase diagram is somewhat different from the one obtained previously[8] with pulsed fields. The reason for this difference is the magnetocaloric cooling discussed in Sec. III C.

The same stability criteria apply to the FL-PM transition with $H||b$ as to the transition between the ordered state and the PM state with $H\perp b$. We, therefore, treat these two boundaries together, and in the following refer to the ordered state with $H\perp b$ also as the FL state. The two boundaries are
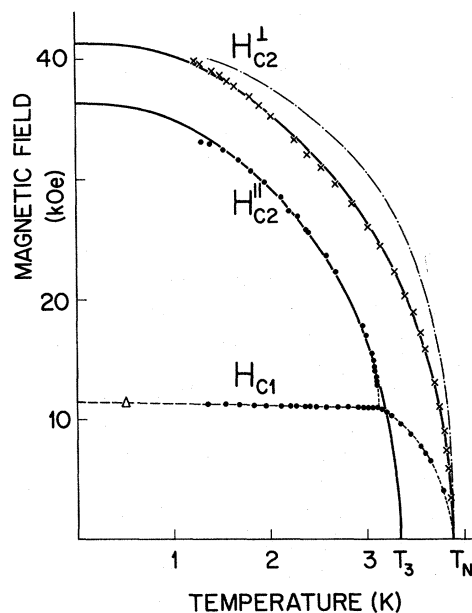

FIG. 4. Isothermal phase diagram of $GdAlO_3$. Dots are field applied along the easy axis b (triangle, Ref. 21); crosses, along c. Solid lines are Brillouin-Weiss curves fitted to the experimental points. Dot-dashes show the temperature dependence of the sublattice magnetization in zero field calculated from the parallel susceptibility.

readily obtained within the MFA from Eq. (1). The instability of the PM state occurs with respect to $\delta\alpha = -\delta\beta$ along the PM-FL boundary. For fields parallel and perpendicular to b the matrix formed by the second derivatives of F decomposes into two 2×2 matrices, and the first eigenvalue to become zero is given by

$$\lambda = F_{\alpha\alpha} - \left| F_{\alpha\beta} \right| = 0 . \tag{7}$$

This yields, for (a) $H\perp b$ $(\alpha = \beta = \tfrac{1}{2}\pi,\ \sigma_A = \sigma_B)$,

$$H_{c2}^{\perp} = (S/g\mu_B)(2J_1 + K_1 - K_2)\,\sigma_\perp(H_{c2}^{\perp}, T) \tag{8a}$$

and, for (b) $H\|b$ $(\alpha = \beta = 0, \sigma_A = \sigma_B)$,

$$H_{c2}^{\|} = (S/g\mu_B)(2J_1 + K_1 + K_2)\,\sigma_\|(H_{c2}^{\|}, T) . \tag{8b}$$

$\sigma_\perp(H_{c2}^{\perp}, T)$ and $\sigma_\|(H_{c2}^{\|}, T)$ are obtained by solving the equilibrium condition $\partial F/\partial\sigma = 0$, which gives

$$\sigma_\perp(H_{c2}^{\perp}, T) = B\{(S^2/T)[(g\mu_B/S)\,H_{c2}^{\perp}(T)$$
$$- (J_1 + J_2)\,\sigma_\perp(H_{c2}^{\perp}, T)]\} , \tag{9a}$$

$$\sigma_\|(H_{c2}^{\|}, T) = B\{(S^2/T)[(g\mu_B/S)\,H_{c2}^{\|}(T)$$
$$- (J_1 + K_1 + J_2)\,\sigma_\|(H_{c2}^{\|}, T)]\} , \tag{9b}$$

and inserting Eqs. (8) into Eqs. (9),

$$\sigma_\perp(H_{c2}^{\perp}, T) = B[(S^2/T)(J_1 + K_1 - J_2 - K_2)\,\sigma_\perp(H_{c2}^{\perp}, T)], \tag{9c}$$

$$\sigma_\|(H_{c2}^{\|}, T) = B[(S^2/T)(J_1 - J_2)\,\sigma_\|(H_{c2}^{\|}, T)] . \tag{9d}$$

Equation (9c) is equivalent to Eq. (3a) for $H = 0$, and therefore

$$\sigma_\perp(H_{c2}^{\perp}, T) = \sigma(0, T) \tag{9e}$$

and, similarly,

$$\sigma_\|(H_{c2}^{\|}, T) = \sigma(0, T\,T_N/T_3) . \tag{9f}$$

Thus, the FL-PM boundaries are Brillouin-Weiss curves. In the case of $H\perp b$ the Brillouin-Weiss curve intercepts the T axis at T_N and the field axis at $H_{c2}^{\perp}(0) = (S/g\mu_B)(2J_1 + K_1 - K_2 - L_0)$, and in the case of $H\|b$ the intercepts are T_3 and $H_{c2}^{\|}(0) = (S/g\mu_B) \times (2J_1 + K_1 + K_2 + L_0)$. The Brillouin-Weiss curves drawn through the experimental points are least-squares fits of the field deviations computed with the intersections on the H and T axes as parameters. They fit the experiment quite well, the standard deviations being 320 Oe for both $H\perp b$ and $H\|b$. The largest deviations from the Brillouin function are found in the region of the triple point, which is determined by the kink in the AF phase boundary as $T_t = 3.12 \pm 0.005$ K [see also Fig. 7(a)]. Here, the measured phase boundary curves away from the Brillouin-Weiss curves and meets the AF phase boundary about 0.1 K below the intersection of the calculated PM boundary with the

measured AF boundary. Minimal standard deviations are obtained for $H\|b$ with the intercepts $H_{c2}^{\|}(T = 0) = 36.28 \pm 0.1$ kOe, $T_3 = 3.35 \pm 0.01$ K; and for $H\perp b$ $(H\|c)$, $H_{c2}^{\perp}(T = 0) = 41.27 \pm 0.1$ kOe, $T_N = 3.878 \pm 0.005$ K. This compares well with previously obtained values from pulsed fields, $H_{c2}^{\|}(T = 0) = 35.5$ kOe and $H_{c2}^{\perp}(T = 0) = 42.0$ kOe. The values reported by Cashion et al.[21] are 7% higher. We believe this discrepancy is mainly due to insufficient compensation for demagnetization as indicated by the finite slope of the M-vs-H curve at the spin-flop transition.

From these isothermal transition fields and a spin-flop field at $T = 0$ K of 11.5 kOe, one obtains, with Eqs. (6), $J_1 = 0.722$ K, $K_1 = 0.0438$ K, and $K_2 + L_0 = -0.0961$ K; furthermore, $T_N - T_3 = \tfrac{1}{3}S(S+1)(K_1 - K_2 - \tfrac{2}{3}L_0)$ yields $L_0 = -0.132$ K and $K_2 = 0.036$ K. The isotropic intrasublattice coupling constant J_2 can then be obtained from either the Néel temperature, the Curie-Weiss θ, or T_3. The Curie-Weiss temperature was obtained from a least-squares fit to previously published[8] susceptibility data in the temperature range from 20 K to liquid N_2 for different field directions perpendicular to b. We found $\theta_\perp = -4.4 \pm 0.4$ K and a Curie constant $C = 7.87$ K/mole, where

$$\theta_\perp = -\tfrac{1}{3}S(S+1)(J_1 + J_2 - \tfrac{2}{9}L_0)$$

is the Curie-Weiss temperature for the perpendicular susceptibility and is different from the commonly used Curie-Weiss temperature $\theta_\|$ for parallel susceptibility as given by Eq. (5b). The value of $\theta_\perp$ used here is somewhat lower than that previously obtained from graphical analysis[8] or from measurements in the liquid-hydrogen temperature range[21] where we find that $1/\chi$ vs T is slightly curved. With the molecular field constants derived above one obtains $J_2 = 0.051$ K from T_N or T_3 and $J_2 = 0.083 \pm 0.07$ K from $\theta_\perp$. For the numerical calculations, however, where $L_0 = 0$, we have used $J_2 = 0.123$ K in order to reproduce the experimental Néel temperature by Eq. (5a). From $\theta_\perp$ and $\theta_\|$, one obtains for the difference of the inverse molar susceptibilities above T_N

$$1/\chi_\| - 1/\chi_\perp = \tfrac{1}{3}(K_1 + K_2 + \tfrac{2}{3}L_0)\,S(S+1)/C,$$

which is independent of temperature. Using the approximation $1/\chi(T_N) \approx 2T_N/C$, the relative difference of the susceptibilities at T_N is

$$\Delta\chi/\chi_\| = (\chi_\perp - \chi_\|)/\chi_\| = S(S+1)(K_1 + K_2 + \tfrac{2}{3}L_0)/6T_N .$$

With the anisotropy constants derived above we obtained $\Delta\chi/\chi_\|(T_N) = -0.05\%$. Experimentally, we could not detect any difference between parallel and perpendicular susceptibility above the Néel temperature within the accuracy of our measurements; Cashion et al.[21] found a small difference of about 1%, but with the opposite sign $(\chi_\| < \chi_\perp)$.

It should be noted that the difference of the suscep-
tibilities is proportional to the difference between
K_1- and K_2- or L_0-type anisotropy fields. (Re-
member that K_1 has to be positive and K_2 and L_0
negative, as is the case in GdAlO$_3$, in order to
favor the same easy direction.) This is in con-
trast to the spin-flop field and the Néel temper-
ature which contain the sum of the anisotropy fields.
This is demonstrated nicely by GdAlO$_3$, where
the total anisotropy is of the order of 20% of the
isotropic exchange, yet no difference of the sus-
ceptibilities is detectable.

The excellent fit of the FL-PM boundaries by
Brillouin-Weiss curves is somewhat surprising.
Combining Eqs. (8a) and (9e), we see that the
transition fields are proportional to the zero-field
sublattice magnetization σ_0, and sublattice mag-
netizations of antiferromagnets do not usually follow
Brillouin-Weiss curves. Since we did not determine
the temperature dependence of σ_0 directly, we cal-
culated σ_0 from the parallel zero-field suscepti-
bility $\chi_{\parallel}$ in order to compare it with H_{c2}. Hornreich
and Shtrickmann[27] have suggested that the MFA re-
lation between $\chi_{\parallel}$ and σ_0 [written here normalized
to $\chi_{\parallel}(T_N)$],

$$\frac{\chi_{\parallel}(T)}{\chi_{\parallel}(T_N)}$$

$$= \frac{6T_N + 2S\,(S+1)\,(J_2+K_2)}{3T_N + 2S\,(S+1)\,(J_2+K_2) + T\,(S+1)/(S\ dB/dX)}\ ,$$

$$(10)$$

where $\sigma_0 = B(X)$, should hold beyond MFA. They
have demonstrated the validity of (10) for a num-
ber of antiferromagnets, where σ_0 does not follow
a Brillouin-Weiss curve at all well. Uncertainties
in the coupling constants J_2 and K_2 are not impor-
tant since $2S\,(S+1)\,(J_2+K_2) \ll 3T_N$. The results of
a numerical solution of Eq. (10) using experimen-
tal values of the zero-field susceptibility are plot-
ted in Fig. 4. The discrepancy between the mea-
sured FL-PM transition fields and those calculat-
ed from the zero-field susceptibility amounts to
as much as 5 kOe, or 20%. As we shall see later,
this discrepancy is due to a change of the sublattice
magnetizations in the FL state, which is not pre-
dicted by MFA.

We further note the validity of the MFA relation
(5c) between the triple point, the Néel temperature,
and T_3, the $H = 0$ intercept of the extrapolated
FL-PM boundary for $H \| b$. With $T_N = 3.875$ K and
$T_t = 3.12$ K, one obtains $T_3 = 3.37$ K, in good agree-
ment with the MFA extrapolation of the FL-PM
boundary.

Consider now the boundary of the AF phase.
Both the transitions to the FL phase and to the
PM phase are no longer simple functions of H and
T and, therefore, have been calculated numeri-

cally. The result of the computation is compared
with experiments in Fig. 5. The agreement is
considerably worse than for the FL-PM phase
boundary. The most striking discrepancy is found
for the spin-flop transition fields near the triple
point; the calculated values of H_{c1} increase from
11.5 kOe at $T = 0$ K to 15.9 kOe at T_t, whereas
the measured transition fields decrease from 11.28
kOe at $T = 1.39$ K to 10.97 kOe at T_t. The calcu-
lated transition field is partially depressed when
L_0-type anisotropy is used. The lower curve has
been calculated with the values of L_0 and K_2 de-
rived above. The calculated transition field of
14.53 kOe, however, is still about 30% too high.
The spin-flop field at higher temperatures could
be further reduced by increasing $|L_0|$ under the
restraint that $L_0 + K_2 = $ const in order to retain the
same critical fields at low temperatures. This
decreases the effective anisotropy at high tem-
peratures, reducing the spin-flop transition field,
but simultaneously pushes the triple point to
higher temperatures.

The temperature dependence of the spin-flop
transition field of GdAlO$_3$ seems to be an excep-
tion. Other well-studied antiferromagnets like
MnF$_2$,[13] Cr$_2$O$_3$,[28] CuCl$_2 \cdot$2H$_2$O,[10,29] NaCrS$_2$,[9]
LiMnPO$_4$,[24] etc., all exhibit an increasing spin-
flop transition field with increasing temperature.
Computations of T_t and the transition field at T_t,
$H_{c1}(T_t)$, with the molecular field constants de-
duced from the transition fields at $T = 0$, and from
T_N and θ, also give better agreement with exper-
iment in these cases. One obtains with K_2-type
anisotropy, for instance, $T_t = 64.6$ K and $H_{c1}(T_t)$
$= 140$ kOe for MnF$_2$, compared with the experi-
mental values of 64.9 K and 119 kOe; and for
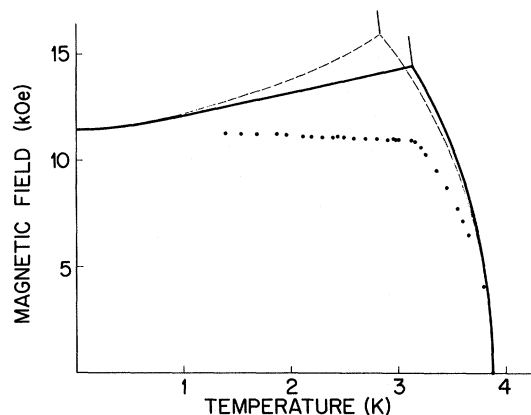CuCl$_2 \cdot$H$_2$O, $T_t = 4.32$ K, $H_{c1}(T_t) = 10.8$ kOe, com-

FIG. 5. Phase boundary of the AF state for fields
applied along the easy axis. Dots are experiment,
dashes calculated with K_2-type anisotropy, and solid
line calculated with K_2-type ($K_2 = +0.036$) and L-type
($L_0 = -0.132$) anisotropy.

pared to $T_t = 4.31$ K and $H_{c1}(T_t) = 8.50$ kOe experimentally. For MnF_2 these values are again improved if L-type anisotropy is used. Then T_t $= 65.4$ K, $H_{c1}(T_t) = 118$ kOe. For $CuCl_2 \cdot 2H_2O$, L-type anisotropy is not effective because of S $= \frac{1}{2}$.

B. Angular Dependence of the Spin-Flop Transition

The existence of a first-order spin-flop transition is not only confined to small angles between the easy axis and the applied field, but extends for finite angles only up to a critical temperature T_c, where it ends in a critical point (Fig. 6). A method well suited to detect the onset of a first-order transition is the soft-mode or truncated-resonance method described by Blazey et al.[23] For finite angles, however, this method is not appropriate here for two reasons. First, the measurable mode, the antiferromagnetic resonance mode, is no longer the soft mode at the spin-flop transition.[5] Second, the field and angular dependence of this AF resonance mode near the spin-flop transition is rather complicated,[5] and cannot be used to identify a metastable region typical for first-order transitions. Here the onset of the first-order spin-flop transition is clearly seen in the susceptibility which exhibits a strong narrow peak. Above the critical temperature the susceptibility has a wider, weaker maximum located along the line connecting the critical point with the kink in the PM-phase boundary at T_t^*. The onset of the first-order transition is then determined from the temperature dependence of the height and width of the susceptibility peak as shown in Fig. 7(a). Above the critical point, the height of the peak decreases and its width increases rapidly with increasing temperature. In this part the temperature variation of both the width and height is independent of the tickling-field frequency.
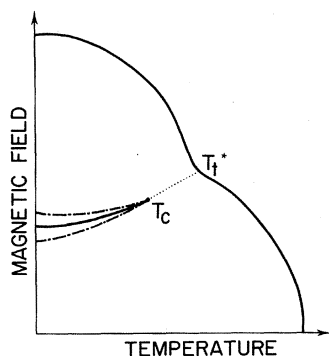

FIG. 6. Schematic phase diagram for H applied at an angle from the easy axis. Dotted line above the critical temperature T_c locates the maximum susceptibility; T_t^* indicates the triple point for $H \parallel b$.
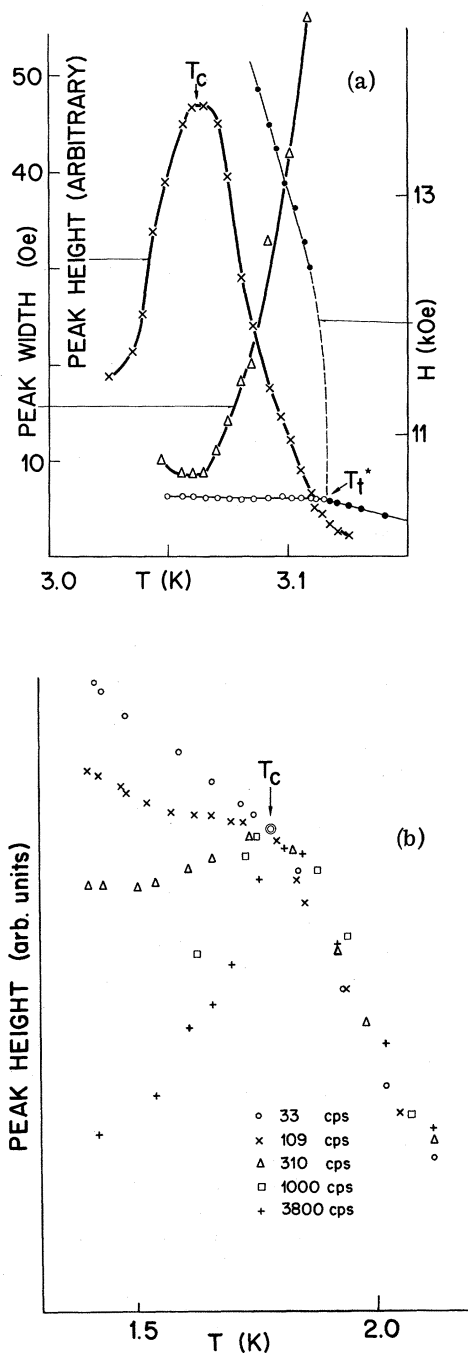

FIG. 7. Determination of the critical temperature with susceptibility peak as function of temperature: (a) Small angle between easy axis and applied field and a modulation frequency of 12 kcps. Crosses show peak height; triangles, peak width; open circles, applied field at the susceptibility peak; solid circles, transition to the PM state. The difference between T_c and T_t^* indicates a misalignment of 0.3 deg. (b) Angle of 5.3 deg between easy axis and applied field. Peak heights for different modulation frequencies have been normalized to 1 at T_c. ⊚ is common to all modulation frequencies.
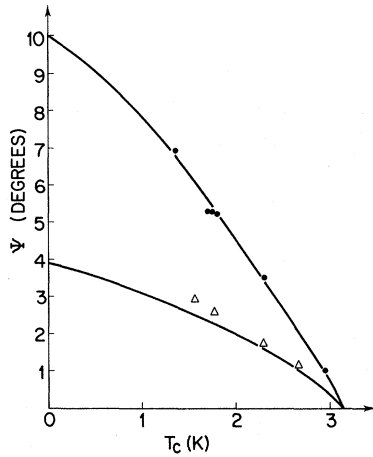
FIG. 8. Critical temperature T_c as function of angle between easy axis and applied field. Solid circles, long cylinders; triangles, disk.

Below the critical point the peak height depends on the modulation-field frequencies as shown in Fig. 7(b). For low frequencies, the peak height continues to increase with decreasing temperature, exhibiting, however, a distinct break in its temperature dependence at the critical point. For intermediate frequencies the peak height remains constant, and for high frequencies, the peak height falls off sharply below the critical point and levels off at very low temperatures. This pronounced frequency dependence comes from two sources. First, low-frequency field modulation means isothermal field changes and the modulation really follows the M-vs-H curve. High frequencies, however, mean adiabatic changes and the modulation sweeps the crystal not through the transition but along the phase boundary, i.e., nearly perpendicular to the M-vs-H curve. Second, minor hysteresis loops, in addition, play a role at the highest frequencies used although no macroscopic hysteresis has been observed. They are probably most important for any further suppression of the signal beyond frequencies comparable with the thermal relaxation of the sample. We found that the most convenient modulation frequency to work with was about 1 kcps. This allowed the determination of the critical temperature with an accuracy of about 0.005 K for small angles, as shown in Fig. 7(a), between easy axis and applied field, and 0.03 K for large angles, in Fig. 7(b).

In Fig. 8, we show the critical temperature as a function of the angle between the easy axis and the applied field, or conversely the critical angle (the angle beyond which a phase transition between the AF state and the FL state no longer exists) as a function of temperature. The curves drawn were obtained by solving the equilibrium and

stability conditions of Eq. (1) numerically. In these computations only K_1- and K_2-type anisotropies could be included. The computed critical temperatures were scaled with $T_t(\text{expt})/T_t(\text{calc})$ in order that the critical temperature for $H \| b$ be equal to the measured triple point. The critical angle for $T = 0$ K was obtained from[4]

$$\tan\psi_{\max}(T = 0) = -\frac{K_2 + L_0}{2J_2 + K_1 + K_2 + L_0}. \qquad (11)$$

The difference between the critical temperatures of the disk and those of the cylinders is due to demagnetizing effects. For small angles between the easy axis and the applied field, the magnetization of a cylindrical sample is, in both the AF state and the FL state, close to the cylinder axis, and at first sight demagnetizing effects would be considered negligible. However, at the transition, the magnetization has to turn first away from the easy direction before lining up again with the easy axis in the other phase. The effect of the accompanying demagnetization on the spin-flop transition is best demonstrated in the simple case of an infinitely long cylinder with easy axis and external field along the cylinder axis. In this case, the magnetization points along the cylinder axis both in the AF and FL state, and all the demagnetizing fields are zero. However, when going from the AF state to the FL state, the instability occurs with respect to $\delta\alpha$, $\delta\beta \neq 0$, which requires that the sublattice magnetizations tilt away from the easy axis and produce a magnetization component perpendicular to the cylinder axis. The resulting perpendicular demagnetizing field in turn exerts a torque on the sublattice magnetizations towards the easy axis thus preventing them from turning away from the easy axis. The instability field is consequently pushed to higher fields; the thermodynamic transition, however, is not affected.

The effect of demagnetization can be incorporated in all the equations by renormalizing the molecular field constants. For an ellipsoid with one of the principal axes along the easy (z) axis, the Zeeman term $-\vec{H} \cdot \vec{M}$ of Eq. (1) can be rewritten in the form

$$F_Z = -\vec{H}_{\text{ext}} \cdot \vec{M} + \tfrac{1}{2}(N_x M_x^2 + N_y M_y^2 + N_z M_z^2), \qquad (12)$$

where the N's are the demagnetizing factors along the principal axis, and the M's, the components of the magnetization. For an antiferromagnet with uniaxial anisotropy the sublattice magnetizations turn in the plane containing the easy axis and the applied field; this is also true for orthorhombic anisotropy as long as the field is perpendicular to the hard direction. If the applied field lies in a principal plane of the demagnetization ellipsoid perpendicular to the hard direction, the magnetization component in the hard direction is always

zero and Eq. (12) becomes

$$F_Z = - \vec{H}_{ext} \cdot \vec{M} + \tfrac{1}{2} [N_{||} (\sigma_A \cos\alpha + \sigma_B \cos\beta)^2$$
$$+ N_\perp (\sigma_A \sin\alpha + \sigma_B \sin\beta)^2] , \quad (12')$$

where $N_{||}$ and $N_\perp$ are the demagnetizing factors in units of energy in this plane $||$ and $\perp$ to the easy axis. The second term of $(12')$ can be redistributed amongst the first four terms of the right-hand side of Eq. (1), leaving the functional form of Eq. (1) unchanged but with renormalized molecular field constants,

$$J_1 \to J_1^* = J_1 + \tfrac{1}{2} N_\perp ,$$

$$J_2 \to J_2^* = J_2 + \tfrac{1}{2} N_\perp ,$$

$$K_1 \to K_1^* = K_1 + \tfrac{1}{2} (N_{||} - N_\perp), \quad (13)$$

$$K_2 \to K_2^* = K_2 + \tfrac{1}{2} (N_{||} - N_\perp),$$

and with the internal field H replaced by the applied field H_{ext}. From the difference of the FL-PM transition for a sphere and a long cylinder, a demagnetizing field of 5.2 kOe for a sphere at full magnetization was obtained, in good agreement with the theoretical value of 5.23 kOe. This gives, for the demagnetizing factors of Eq. (13), $N_\perp = 0.300$ K for the long cylinder, and $N_{||} = N_\perp = 0.0072$ K for the disk used in the present experiment.

In the case of the disk, the critical angle is practically not influenced by the demagnetization, whereas in the case of the cylinder, the critical angle is nearly tripled due to $N_\perp$. This is well verified by the experiment. The small systematic deviations of the critical temperatures of the disk are attributed to uncertainties in the K_2- and L-type anisotropies and to possible misalignment of the disk plane away from the applied field. The K_2- or L-type anisotropy, which determines the critical angle, is experimentally obtained from the difference of two large quantities obtained by extrapolation of the phase diagram to zero temperature. A possible error of 10% in K_2 would account for the observed deviations. Moreover, L-type anisotropy in place of K_2-type anisotropy would also alter the calculations somewhat. These arguments do not apply for the cylinder because there the dominant part of the anisotropy which determines the critical angle is of K_2-type owing to demagnetization and is well known. In case of misalignment of the disk plane, the sublattice magnetizations no longer lie in the disk plane. The orthorhombic nature of the anisotropy induced by the axial shape anisotropy then plays a vital role for the equilibrium positions of the sublattice magnetizations, and the critical angle depends on the

anisotropy along the hard direction.

C. Magnetocaloric Effects

The phase diagram with the field applied along the easy axis measured in the present investigation is compared with that obtained previously[8] in pulsed fields in Fig. 9. The apparent difference between the two phase diagrams occurs because, during the pulsed-field experiment, the crystal cools upon adiabatic magnetization in the AF phase. The temperatures plotted are those at the start of the field pulse and not those at which the transition occurs. Connected with the adiabatic cooling is an entropy increase upon isothermal magnetization in the AF phase. The origin of this entropy increase is illustrated in Fig. 10 for the case $H || b$. According to Eq. (2), the entropy decreases monotonically with increasing sublattice magnetization. On turning on a field, the sublattice magnetization σ_A, which is parallel to the field, increases and σ_B decreases with the same initial slopes. Thus the isentropes in an H-T diagram leave the T axis with infinite slope as required, since the line $H = 0$ is not a phase boundary. As the field is further increased, σ_B decreases faster than σ_A increases and the total entropy increases. At the spin-flop transition the entropy increases or decreases discontinuously, depending on the temperature dependence of the transition field. In our calculations, H_{c1} increases with increasing temperature (see Fig. 5) and the entropy decreases when crossing the phase boundary. Experimentally, however, H_{c1} decreases slightly with temperature. In the adiabatic case,
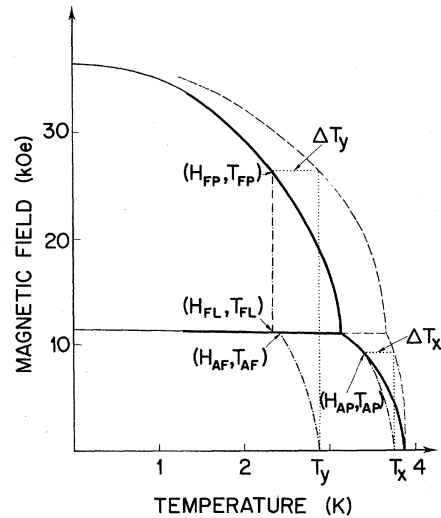
FIG. 9. Comparison of isothermal (solid lines) and adiabatic (dashed lines) phase diagrams for the field applied along the easy axis. Dash-dots show isentropes of the isothermal phase diagram. Amount of adiabatic cooling between $H = 0$ and the PM phase boundary is shown by ΔT_x and ΔT_y.
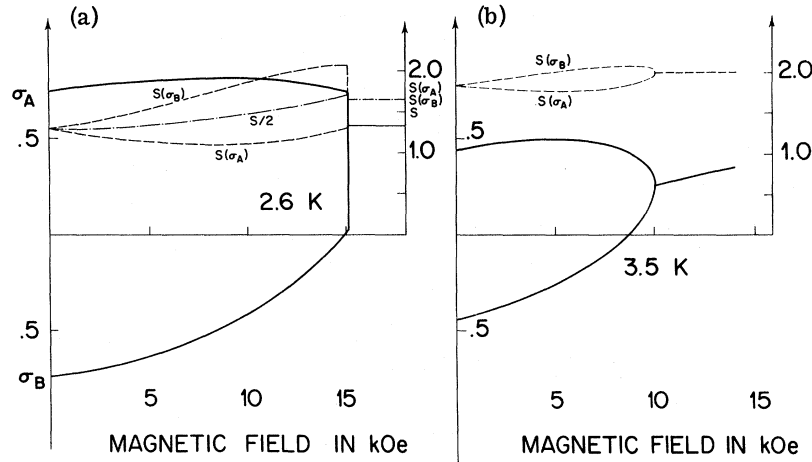
FIG. 10. Variation of the calculated sublattice magnetization and entropy with magnetic field (a) below and (b) above the triple point.

starting at a temperature T_x, the sample cools down to T_{AP} on magnetization where the AF-PM phase boundary is met at a field H_{AP}. Starting at a lower temperature T_y, the temperature decreases to T_{AF} where the AF-FL phase boundary is met at a field H_{AF}. Owing to the latent heat, the isentrope coincides with the phase transition down to a state (H_{FL}, T_{FL}). In the flop state, the sublattice magnetization is independent of field [Eq. (3b)] and the temperature stays constant until the FL-PM phase boundary is met at (H_{FP}, T_{FP}). The phase diagram obtained by plotting the transition fields H_{AF}, H_{FL}, H_{FP}, and H_{AP} as functions of the temperatures T_{AF}, T_{FL}, T_{FP}, and T_{AP}, respectively, is of course identical to the isothermal one. Since in our pulsed field experiment these temperatures are not known, we shall refer in the future to the plot of these transition fields as a function of the temperature at the start of the field pulse $(T_x$ and T_y in Fig. 9) as the adiabatic phase diagram, which is then different from the isothermal one.

Consider first those aspects of the adiabatic cooling connected with the phase diagrams. From the difference of the adiabatic and isothermal phase diagrams, we obtain the total cooling when going from $H=0$ to the PM phase boundary. The lattice contribution to the total entropy can be neglected and then the entropy is a function of the sublattice magnetizations alone. We have then

$$\sigma_A(0, T_x) = \sigma_P(H_{AP}, T_{AP}) \qquad (14a)$$

and

$$\sigma_A(0, T_y) = \sigma_{FL}(H_{FL}, T_{FL}) = \sigma_P(H_{FP}, T_{FP}) . \qquad (14b)$$

Rewriting Eqs. (3) in the form

$$\sigma_A(0, T) = B\left(\frac{3S}{S+1} \sigma_A(0, T) \frac{T_N}{T}\right)$$

$$= B[X_A(0, T)] , \qquad (15a)$$

$$\sigma_{FL}(H_{FL}, T_{FL}) = B\left(\frac{3S}{S+1} \sigma_{FL}(H_{FL}, T_{FL}) \frac{T_3}{T_{FL}}\right)$$

$$= B[X_{FL}(H_{FL}, T_{FL})], \qquad (15b)$$

$$\sigma_P(H_{AP}, T_{AP})$$

$$= B\left[\left(g\mu_B SH - \frac{3S}{S+1} \sigma_P(H_{AP}, T_{AP})\theta_{\shortparallel}\right)\Big/ T_{AP}\right]$$

$$= B[X_P(H_{AP}, T_{AP})] , \qquad (15c)$$

where T may equal T_x or T_y, conditions (14) are equivalent to

$$X_A(0, T_x) = X_P(H_{AP}, T_{AP}), \qquad (14c)$$

$$X_A(0, T_y) = X_{FL}(H_{FL}, T_{FL}) = X_P(H_{FP}, T_{FP}). \qquad (14d)$$

The cooling for the case where the isentrope cuts the PM boundary below T_t is readily obtained by comparing (15a) and (15b), which yield

$$T_N/T_y = T_3/T_{FL} . \qquad (16a)$$

The cooling, expressed in measurable quantities, is then

$$\Delta T_y = T_y - T_{FL}$$

$$= T_y(T_N - T_3)/T_N$$

$$= \frac{2}{3} T_y(T_N - T_t)/T_N . \qquad (16b)$$

The cooling decreases linearly with decreasing temperature. The maximum temperature $T_{y,max}$ up to which Eq. (16b) holds is obtained by setting $T_{FL} = T_t$ in Eq. (16a). This gives, to first order in $(T_N - T_t)/T_N$,

$$T_{y,max} = T_N T_t/T_3 = \frac{1}{3}(2T_N + T_t) . \qquad (16c)$$

At this temperature the cooling is

$$\Delta T_{y,\max} = T_t(T_N - T_3)/T_3 = \tfrac{2}{3}(T_N - T_t) \quad . \quad (16d)$$

For the case where the isentrope cuts the PM phase boundary above T_t, we first have to calculate the phase boundary. At this phase boundary, the PM state becomes unstable with respect to $\delta\sigma_A = -\delta\sigma_B$. The relevant eigenvalue is then given by

$$\lambda = (F_{\sigma_A\sigma_A} - |F_{\sigma_A\sigma_B}|)_{\sigma_A = \sigma_B = \sigma_P} = 0. \quad (17)$$

This yields

$$S^2(J_2 + K_2) + T/[dB(X_P)/dX_P] - S^2|J_1 + K_1| = 0, \quad (17')$$

where we have made use of the following relation:

$$d^2s(\sigma_P)/d\sigma_P^2 = dB^{-1}(\sigma_P)/d\sigma_P$$

$$= \frac{dB^{-1}(\sigma_P)}{dX_P}\,\frac{dX_P}{d\sigma_P} = \frac{1}{dB(X_P)/dX_P} \quad ,$$

where $\sigma_P = B(X_P)$. If we expand $dB(X)/dX$ in powers of X,

$$\frac{dB(X)}{dX} = \frac{S+1}{3S} - 3aX^2 \ , \quad (18)$$

where $a = \tfrac{1}{45}[(2S+1)^4 - 1]/(2S)^4$, we obtain for X_P along the AF-PM boundary

$$X_P^2(H_{AP}, T_{AP}) = \frac{S+1}{3S}\,\frac{T_N - T_{AP}}{3aT_N} \ . \quad (19)$$

Expanding Eq. (15a) yields

$$X_A^2(0, T_X) = \frac{S+1}{3S}\,\frac{T_N - T_x}{aT_N} \ .$$

Setting $X_A^2 = X_P^2$ gives

$$\tfrac{1}{3}(T_N - T_{AP}) = (T_N - T_x) \ , \quad (20a)$$

and a cooling

$$\Delta T_x = T_x - T_{AP} = 2(T_N - T_x) \quad . \quad (20b)$$

The cooling increases linearly with decreasing temperature. The minimum temperature $T_{x,\min}$, down to which Eq. (20b) holds, is again obtained by replacing T_{AP} by T_t in Eq. (20a):

$$T_{x,\min} = \tfrac{1}{3}(T_t + 2T_N) \ , \quad (20c)$$

which is of course equal to $T_{y,\max}$. Also the maximum cooling $\Delta T_{x,\max}$ is the same as that derived previously for $\Delta T_{y,\max}$. Note that Eq. (5c) relating T_N, T_3, and T_t can be obtained by equating $T_{y,\max} = T_N T_t/T_3$ and $T_{x,\min} = \tfrac{1}{3}(T_t + 2T_N)$.

Thus the adiabatic cooling between the state $H = 0$ and the PM phase boundary increases linearly with decreasing temperature to a maximum value of $\tfrac{2}{3}(T_N - T_t)$ at $T = \tfrac{1}{3}(T_t + 2T_N)$. The cooling between $H = 0$ and the flop state decreases linearly from this maximum value to zero at $T = 0$ K. In Fig. 11, we compare the calculated adiabatic cooling with experiment for GdAlO$_3$ and CuCl$_2 \cdot$ 2H$_2$O. In the

case of GdAlO$_3$, the calculated maximum cooling is 0.51 K at $T = 3.63$ K. The experiment agrees very well with the calculations above the triple point. Below the triple point, however, a direct comparison between calculation and experiment is not possible. With K_2-type anisotropy, no cooling is calculated for the flop state, yet experimentally, considerable cooling is observed, as can be seen from comparing the steady-field and pulsed-field phase boundary when the field is applied perpendicular to the easy axis as shown in Fig. 12. The cooling ΔT given by Eq. (16b) is then no longer equal to the total measured cooling ΔT_m between the state $H = 0$ and the PM phase boundary, but has to be compared with

$$\Delta T = \Delta T_m - \delta T \ ,$$

where δT is the cooling in the FL state. We have estimated δT by assuming it proportional to the applied field, as was found experimentally in the case of CuCl$_2 \cdot$ 2H$_2$O.[10] If we further assume that the cooling in the FL state is the same for $H \parallel b$ and $H \perp b$, we obtain for δT

$$\delta T(T) = \Delta T_\perp \left(T\,\frac{T_3}{T_N}\right)\,\frac{H_{c2}(T) - H_{c1}(T)}{H_{c2}(T)} , \quad (21)$$

where $\Delta T_\perp$ is the measured cooling between $H = 0$ and $H = H_{c2}^\perp$ with the field applied perpendicular to the easy axis. The remaining discrepancy between experiment and calculation at low temperatures is due to an anisotropic component of the cooling in the FL state as shown later.

In the case of CuCl$_2 \cdot$ 2H$_2$O, Butterworth and Zidell[10] have measured the isentropes and ΔT is directly obtained from their measurements. The
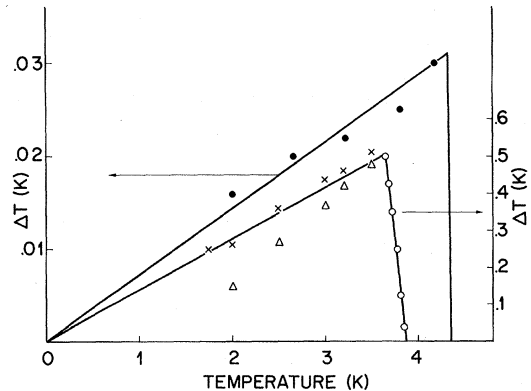

FIG. 11. Adiabatic temperature change in the AF state plus that on going through the spin-flop transition as function of the initial temperature. GdAlO$_3$: circles, no correction; triangles, correction for isotropic cooling in the FL state; crosses, correction for anistropic cooling in the FL state. CuCl$_2 \cdot$ 2H$_2$O: solid circles. The solid lines are the adiabatic cooling obtained from Eqs. (16b) and (20b).
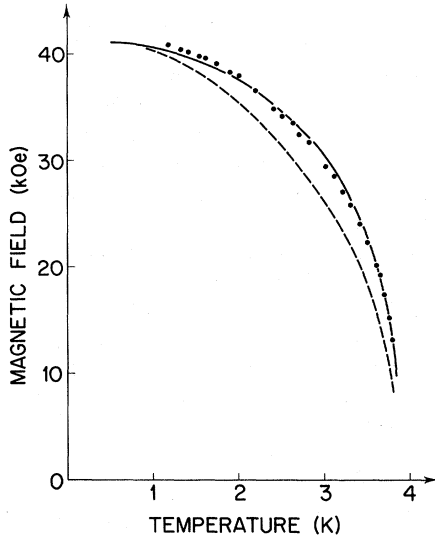
FIG. 12. Comparison of the PM phase boundary for field perpendicular to the easy axis ($H \parallel c$) with the sublattice magnetization computed from the parallel susceptibility by Eq. (10). Dashed lines are isothermal boundary; solid circles, adiabatic boundary; the solid line represents the sublattice magnetization normalized to 41.27 at $T = 0$ K computed from the susceptibility results of Refs. 8 and 21.

experimental accuracy permits only a comparison with the calculation below the triple point. In this region the ΔT to be compared with that of Eq. (16b) is the total cooling in the AF phase plus the heating at the phase transition. Also in this case, the agreement is quite satisfactory.

The observed adiabatic cooling in the flop state with $H \perp b$ indicates that the sublattice magnetizations in the FL state decrease with isothermally increasing field. In a pulsed-field experiment (adiabatic process), however, the magnitude of the sublattice magnetizations remains constant. Then for fields perpendicular to the easy direction, the adiabatic FL-PM phase boundary should, according to Eq. (8), exhibit the same temperature dependence as the zero-field sublattice magnetization. We tested this in Fig. 12, where we have plotted the adiabatic transition field and the sublattice magnetization obtained from $\chi_\parallel$ as a function of temperature. The good agreement between the adiabatic FL-PM phase boundary and the zero-field sublattice magnetization verifies Eq. (8), which relates the FL-PM phase boundary to the sublattice magnetization at the boundary. A possible source of the isothermal reduction of the sublattice magnetization in the FL state with $H \perp b$ and the adiabatic cooling associated with it is molecular fields which are not linear in σ as, for example, L-type anisotropy. Including L-type anisotropy, Eq. (3d) becomes

$$\sigma = B \left\{ \frac{S^2}{T} \ \sigma \left[J_1 + K_1 - J_2 - K_2 \right. \right.$$

$$\left. \left. - L_0 \left(\tfrac{2}{3} l(\sigma) + \tfrac{1}{2} (\cos^2 \varphi - \tfrac{1}{3}) \sigma \frac{dl}{d\sigma} \right) \right] \right\} ,$$

where the field dependence of σ is caused by the term $\cos^2 \varphi$, and is

$$\frac{d\sigma}{dH} = \frac{dB}{dX} \frac{dX}{dH} \propto - \frac{L_0 d \cos^2 \varphi}{dH} \frac{dl}{d\sigma} \frac{dB}{dX} .$$

Since $L_0 < 0$, $d(\cos^2 \varphi)/dH < 0$, $dl/d\sigma > 0$, and $dB/dX > 0$, one obtains $d\sigma/dH < 0$, i.e., the sublattice magnetizations decrease with increasing field as required. If the field is applied parallel to b, Eq. (3b) becomes

$$\sigma = B \left\{ \frac{S^2}{T} \ \sigma \left[J_1 - J_2 + L_0 \left(\tfrac{1}{3} l(\sigma) - \tfrac{1}{2} (\cos^2 \varphi - \tfrac{1}{3}) \sigma \ \frac{dl}{d\sigma} \right) \right] \right\} .$$

Since in this case $d(\cos^2 \varphi)/dH > 0$, one obtains $d\sigma/dH > 0$, i.e., the sublattice magnetizations increase with increasing field and the sample heats on adiabatic magnetization. The computed isothermal reduction and adiabatic cooling for $H \perp b$, and for the anisotropy constants $L_0 = -0.132$ K and $K_2 = 0.036$ K, are about a factor four smaller than found experimentally, and the computed heating for $H \parallel b$ is nearly equal to the computed cooling for $H \perp b$. Thus the dominant cause for the change of magnitude of the sublattice magnetization in the FL state is not contained in MFA. If we assume that the total cooling in the FL state is due to a large isotropic non-MFA component and a cooling or heating due to L-type anisotropy, then the total cooling in the FL state for $H \parallel b$ is about half of that given by Eq. (21). This reduced correction leads to good agreement for the total cooling between the $H = 0$ state and the FL state, as can be seen from Fig. 11. The source of the isotropic cooling in the FL state is not known at present.

The field dependence of the magnitude of the sublattice magnetizations in the FL state might be expected to induce some field dependence in the susceptibility χ. The magnetization in the direction of the applied field perpendicular and parallel to the easy axis is

$$M \left(\substack{\perp \\ \parallel} \right) = \frac{g \mu_B H / S}{2 J_1 + K_1 \mp K_2 \mp L_0 l(\sigma)} \approx \frac{H}{AG} \left[1 \pm \delta l(\sigma) \right] ,$$

where the upper signs refer to $M_\perp$ and the lower signs to $M_\parallel$, $G = 2J_1 + K_1 \mp K_2$, and $\delta = L_0 / G$. The change of χ is then

$$d\chi \left(\substack{\perp \\ \parallel} \right) \Big/ dH = d^2 M \left(\substack{\perp \\ \parallel} \right) \Big/ dH^2 \approx \pm \frac{\delta}{AG} \frac{dl}{d\sigma} \frac{d\sigma}{dH} ,$$

where terms containing $d^2 l / d\sigma^2$ and $d\sigma^2 / dH^2$ have been neglected. Since $\delta < 0$, $1 > dl/d\sigma > 0$, and $d\sigma/$

$dH < 0$ for $H \perp b$, and $d\sigma/dH > 0$ for $H \parallel b$, the relative change of χ is at least an order of δ smaller than that of σ, and χ increases with increasing field whether σ increases or decreases. The computed total change of χ is at most 0.3% compared to a maximal change of σ of 4%. Experimentally, the parallel susceptibility in the FL state is practically field independent, except close to the transitions where χ increases rapidly (see Fig. 3). Since the same field dependence of χ in the FL state is found both in isothermal and adiabatic[8] experiments, it is not connected with an entropy change and, in particular, not due to changes in the sublattice magnetizations responsible for adiabatic cooling in the FL state. It has been suggested[9,25] that the increase of susceptibility near the FL-PM transition might be due to the freezing out of the zero-point motion. The increase of the sublattice magnetization due to this effect is of course not connected with an entropy change, since the zero-point motion does not contain any entropy and should, therefore, be observed both isothermally and adiabatically. The excess susceptibility just above the transition is of the same order as that below the transition and cannot be attributed to zero-point motion effects. As an alternative explanation we suggest that critical fluctuations are responsible for the strong field dependence of χ near the FL-PM transition. The fact that the extra susceptibility is also seen in pulsed-field experiments points to fluctuations in the angle between the sublattices, in agreement with the type of instability occurring at the FL-PM boundary.

L-type anisotropy also changes the temperature dependence of the FL-PM transitions slightly as given by Eqs. (8) and (9). The transition fields are no longer proportional to the sublattice magnetization at the transition, and this sublattice magnetization no longer follows a Brillouin-Weiss curve. However, these changes are small ($< 3\%$) and nearly compensate, so that the FL-PM boundary computed with L-type anisotropy deviates by less than 1% from a Brillouin-Weiss curve.

Finally, we note that the magnetocaloric effect in the paramagnetic state is the cause of the reduced saturation magnetization observed in the adiabatic magnetization curves.[8] In the paramagnetic phase the change of magnetization is connected with equal changes of the sublattice magnetizations and thus with a change of entropy. At low temperatures where the temperature dependence of the lattice entropy is negligible compared to that of the spin system, the total magnetization cannot change in an adiabatically increasing field and the sample heats according to $H/T = $ const. On heating sufficiently the lattice starts to absorb some of the spin entropy and consequently the magnetization increases again. This explains the plateau observed

in the magnetization after entering the paramagnetic phase in the pulsed-field experiments.[8] The increase in magnetization immediately after the PM phase boundary observed in these experiments is caused by the excess susceptibility attributed to the fluctuations in the neighborhood of the phase transition.

D. Behavior of the Phase Diagrams near T_N

Finally, we consider the behavior of the phase diagram near the Néel point. In MFA, all the PM transition fields H_{c2} vary as $[(T_N - T)/T_N]^{1/2}$ near T_N.[13,30] Near T_N, σ is small and we set $l(\sigma) \approx l(0) = \frac{2}{3}$ and $dl/d\sigma = 0$. Then $H_{c2}^{\perp}$ is proportional to $\sigma(H = 0)$. Expanding $\sigma(H = 0) = B[3S\sigma T_N/(S+1)T]$ in powers of $3S\sigma T_N/(S+1)T$ gives $\sigma \sim \epsilon^{1/2}$, where $\epsilon = (T_N - T)/T_N$, and thus $H_{c2}^{\perp} \propto \epsilon^{1/2}$, the proportionality constant being $A(2J_1 + K_1 - K_2 - \frac{2}{3}L_0)(T/T_N)\{[(S+1)/3S]^3/a\}^{1/2}$, where $a = \frac{1}{15}[(2S+1)^4 - 1]/(2S)^4$. For the reduced critical field $h_{c2}^{\perp} = H_{c2}^{\perp}/H_{c2}^{\perp}(T = 0)$, we then obtain

$$h_{c2}^{\perp} = \varphi(S)\epsilon^{1/2}(1 - \epsilon)(1 + \Delta_{\perp}), \tag{22}$$

where $\varphi(S)$ is a function of the spin alone, $\varphi(S) = 1.44$ for $S = \frac{7}{2}$, and $\Delta_{\perp} = \frac{1}{3}L_0/(2J_1 + K_1 - K_2 - L_0) = -0.03$, a small correction due to L-type anisotropy.

For $H \parallel b$, the equilibrium condition $F_\sigma = 0$ gives

$$\sigma(J_1 + K_1 + J_2 + K_2) - H/A + XT/S^2 = 0,$$

where again $X = B^{-1}(\sigma) = -ds(\sigma)/d\sigma$. Expanding $\sigma = B(X)$ in powers of X, one obtains

$$X = HS^2/[A(T - \theta)].$$

Setting X equal to X_P of Eq. (19) immediately gives $H_{c1}^{\parallel} \propto \epsilon^{1/2}$, where the proportionality constant is $\sqrt{3}A\varphi(S)(T - \theta_{\parallel})/S(S+1)$. For the reduced critical field we obtain

$$h_{c2}^{\parallel} = \frac{1}{3}\sqrt{3}\varphi(S)\epsilon^{1/2}[1 - \frac{1}{2}(\delta + \epsilon)](1 + \Delta_{\parallel}), \tag{22'}$$

where again $\delta = -2(J_2 + K_2 + \frac{4}{9}L_0)/(J_1 + K_1 - J_2 - \frac{4}{9}L_0)$ and $\Delta_{\parallel} = -(2J_2 - K_1 + 3K_2 + \frac{17}{9}L_0)/(2J_1 + K_1 + K_2 + L_0)$ are corrections; for GdAlO$_3$, $\delta = 0.18$ and $\Delta_{\parallel} = +0.20$. Equations (22) and (22') are essentially the "law of corresponding states" given by Foner and Shapira.[13] Experimentally, we find for the exponents β and the proportionality factors b defined by $h_{c2}^{\perp}/[(1 - \epsilon) \times (1 + \Delta_{\perp})] = b_{\perp}\epsilon^{\beta_{\perp}}$ and $h_{c2}^{\parallel}/\{[1 - \frac{1}{2}(\epsilon + \delta)](1 + \Delta_{\parallel})\} = b_{\parallel}\epsilon^{\beta_{\parallel}}$

$$\beta_{\perp} = 0.51 \pm 0.02, \quad b_{\perp} = 1.67 \pm 0.1,$$

$$\beta_{\parallel} = 0.51 \pm 0.02, \quad b_{\parallel} = 0.73 \pm 0.05,$$

in the interval $5 \times 10^{-3} < \epsilon < 0.12$, compared to the MFA values $\beta_{\perp} = \beta_{\parallel} = 0.5$, $b_{\perp} = 1.44$, and $b_{\parallel} = 0.83$. Foner and Shapira[13] observed the same temperature dependence of the PM transition near T_N in MnF$_2$ and FeF$_2$. The values of β close to $\frac{1}{2}$ reflect

the molecular field behavior of the PM phase boundary. Also interesting is the behavior of the adiabatic phase diagram near T_N. The adiabatic transition fields for $H \perp b$ should be proportional to the zero-field sublattice magnetization and, therefore, reflect the behavior of the order parameter near T_N. We find for β and b, now defined by $h_{c2} = b \epsilon^\beta$,

$$\beta_\perp = 0.36 \pm 0.02 , \quad b_\perp = 1.20 \pm 0.1 ,$$

$$\beta_\parallel = 0.31 \pm 0.02 , \quad b_\parallel = 0.70 \pm 0.05 ,$$

in the temperature interval $10^{-2} < \epsilon < 1.2 \times 10^{-1}$ for $H \perp b$ and $5 \times 10^{-3} < \epsilon < 7.10^{-2}$ for $H \parallel b$. The values of $\beta_\perp$ and $b_\perp$ are in good agreement with those found in other antiferromagnets for the critical behavior of the zero-field sublattice magnetization.[30] Thus the sublattice magnetization σ_0 along the line $H = 0$ exhibits the critical behavior expected from an order parameter, whereas the sublattice magnetization along the PM phase boundary is correctly given by MFA. The critical phenomena of the susceptibility near the FL-PM transition and of the transition fields near T_N are being investigated further.

IV. SUMMARY

Here, the isothermal magnetic phase diagram of $GdAlO_3$ has been determined from differential magnetization measurements for various angles between easy axis and applied field. From the phase diagram for fields parallel and perpendicular to the easy axis we have determined all the molecular field constants. The difference between these phase diagrams and the adiabatic ones demonstrates vividly the expected magnetocaloric cooling of an antiferromagnet upon adiabatic magnetization.

Most of the properties of the phase diagram can be accounted for in the molecular field approximation, the most important features being the following: (a) The FL-PM transition fields are practically proportional to the sublattice magnetization at the transition. (b) The isothermal FL-PM boundaries follow the expected Brillouin-Weiss curves in spite of an extra field dependence of the sublat-

tice magnetization in the FL state not contained in MFA. (c) The adiabatic FL-PM boundary is proportional to the zero-field sublattice magnetizations which are different from their molecular field values. (d) The first-order spin-flop transition is found to be restricted to small angles between easy axis and applied field in good agreement with theory. (e) The critical angle and the critical temperature are very sensitive to demagnetizing fields, e.g., the critical angle of a cylinder is nearly three times that of a disk. Contrary to the calculations and experimental results on other well-studied antiferromagnets, the spin-flop transition field increases with decreasing temperature.

The molecular field adiabatic cooling in the antiferromagnetic state increases linearly in temperature to a maximum value when the final temperature is at the triple point, and afterwards decreases linearly to zero at the Néel temperature in good agreement with experiment. In the flop state, adiabatic cooling for fields perpendicular to the easy axis and heating for fields parallel to the easy axis are expected due to the special field dependence of the L-type anisotropy. Experimentally, however, an over-all cooling is observed due to a large additional isotropic cooling which cannot be accounted for in MFA.

The transition to the PM phase near T_N for fields parallel and perpendicular to the easy axis is well described by MFA and obeys the law of corresponding states. In the adiabatic case, where the PM transition field for $H \perp b$ is proportional to the zero-field sublattice magnetization, the same critical behavior near T_N is found as in other antiferromagnets.

*Present address: Department of Physics, University of Bristol, England.

[1]C. J. Gorter and Tineke van Peski-Tinbergen, Physica 22, 273 (1956); Yung-Li Wang and H. B. Callen, J. Phys. Chem. Solids 25, 1459 (1964); F. B. Anderson and H. B. Callen, Phys. Rev. 136, A1068 (1964).

[2]J. Feder and E. Pytte, Phys. Rev. 168, 640 (1968).

[3]G. K. Chepurnkh, Fiz. Tverd. Tela 10, 1917 (1968) [Sov. Phys. Solid State 10, 1517 (1968)]; M. J. Kaganov and G. K. Chepurnykh, Fiz. Tverd. Tela 12, 2988 (1970) [Sov. Phys. Solid State 11, 745 (1969)].

[4]H. Rohrer and H. Thomas, J. Appl. Phys. 40, 1025 (1969).

[5]H. Thomas, in Proceedings of the Chania International Conference on Magnetism, Crete, 1969 (Gordon and Breach, New York, to be published), Vol. 8; K. W. Blazey, M. Ondris, H. Rohrer, and H. Thomas, J. Phys. (Paris) 32, 1020 (1971); H. Rohrer and H. Thomas (unpublished).

[6]W. E. Henry, Phys. Rev. 94, 1146 (1954).

[7]J. E. Rives, Phys. Rev. 162, 491 (1967).

[8]K. W. Blazey and H. Rohrer, Phys. Rev. 173, 574 (1968).

[9]K. W. Blazey and H. Rohrer, Phys. Rev. 185, 712 (1969).

[10]G. J. Butterworth and V. S. Zidell, J. Appl. Phys. 40, 1033 (1969).

[11]G. J. Butterworth, V. S. Zidell, and J. A. Woollam, Phys. Letters 32A, 24 (1970).

[12]J. H. Schelling and S. A. Friedberg, Phys. Rev. 185, 728 (1969).

[13]Y. Shapira and S. Foner, Phys. Rev. B 1, 3083 (1970); Y. Shapira, ibid. 2, 2725 (1970).

[14]K. W. Blazey and H. Rohrer, in Proceedings of the Conference on High Magnetic Fields and Their Applications, Nottingham, 1969, Booklet 1, p. 108 (unpublished).

[15]K. W. Blazey, H. Rohrer, and R. Webster, in Proceedings of the Conference on High Magnetic Fields and Their Applications, Nottingham, 1969, Booklet 1, p. 109 (unpublished).

[16]N. Kurti, J. Phys. Radium 12, 281 (1951).

[17]W. P. Wolf, Phys. Rev. 115, 1196 (1959).

[18]A. E. Clark and Earl Callen, Phys. Rev. Letters 23, 307 (1969).

[19]H. J. Scheel and E. O. Schulz-DuBois, J. Cryst. Growth 8, 304 (1971).

[20]S. Geller and B. Bala, Acta Cryst. 9, 1019 (1956).

[21]J. D. Cashion, A. H. Cooke, T. L. Thorp, and M. R. Wells, Proc. Roy. Soc. (London) A318, 473 (1970).

[22]H. Goldstein, S. J. Williamson, and S. Foner, Rev. Sci. Instr. 36, 1356 (1965).

[23]K. W. Blazey, K. A. Müller, M. Ondris, and H. Rohrer, Phys. Rev. Letters 24, 105 (1970).

[24]I. S. Jacobs, J. Appl. Phys. 32, 619 (1961); J. H. Rainicar and P. R. Elliston, Phys. Letters 25A, 720 (1967).

[25]I. S. Jacobs and S. D. Silverstein, Phys. Rev. Letters 13, 272 (1964).

[26]J. Kanamori and K. Yosida, Progr. Theoret. Phys. (Kyoto) 14, 423 (1955).

[27]R. Hornreich and S. Shtrickmann, Phys. Rev. 159, 408 (1967).

[28]S. Foner and Shou-Ling Hou, J. Appl. Phys. 33, 1289 (1962).

[29]N. J. Poulis and G. E. G. Hardeman, Physica 20, 7 (1954).

[30]P. Heller, Rept. Progr. Phys. XXX, 731 (1967).

Infrared Absorption and Raman Scattering by Two-Magnon Processes in NiO

R. E. Dietz, G. I. Parisot,* and A. E. Meixner

Bell Telephone Laboratories, Murray Hill, New Jersey 07974

(Received 29 April 1971)

Strong two-magnon (2M) Raman scattering has been observed from NiO along with first- and second-order phonon scattering. The shape of the 2M scattering peak is well described by a simple-cubic Green's function for interacting spin waves with an intersublattice exchange J_2 = 148 cm^{-1}. The temperature shift of the scattering peak is identical to that of the 2000-cm^{-1} ir absorption peak described by Newman and Chrenko, but energy considerations require the absorption peak to be a phonon sideband of the 2M scattering peak, which is not seen in absorption.

I. INTRODUCTION

NiO has been widely investigated as a model magnetic semiconductor, and a candidate for a metal-insulator transition which has never been found. While much work has been done on its optical and electrical properties, little quantitative information has been available concerning the exchange interactions leading to its antiferromagnetic order and the resulting magnetic excitations. Furthermore, a strong, temperature-dependent absorption band is observed[1] near 2000 cm^{-1} which has variously been interpreted as the excitation of a zone-boundary magnon and a phonon $(M+P)$,[1] two zone-boundary magnons $(2M)$,[1] and the simultaneous excitation of two magnons and a phonon $(2M+P)$,[2] among other suggestions.

In this paper we study the exchange interactions in NiO by observing the two-magnon $(2M)$ Raman scattering in both halide-vapor-decomposition-grown crystals (called "green" NiO because of its

transparency in thin sections) and also in "black" crystals containing excess oxygen, grown by the flame-fusion technique. In order to choose among the various mechanisms so far proposed to account for the ir band, we measure the temperature dependence of the Raman scattering between 1.4 and 600 °K, and compare this to the ir data of Newman and Chrenko[1] above room temperature, which we supplement with low-temperature absorption data.

II. EXPERIMENT

The experiments were performed on samples of uncertain origin. However, some of the crystals were believed to have been grown by epitaxial vapor deposition on MgO, presumably by the decomposition of the halide.[3] These crystals were thin (200 μ thick) platelets oriented with (100) faces, and exhibited no detectable absorption between 3000 and 6000 cm^{-1}. The "black" crystals were cut into similar (100) slabs about 100 μ thick. All crystals were polished with a 3-μ diamond paste on a tin